ACS OMEGA

Open Access

http://pubs.acs.org/journal/acsodf

Article

Self-Assembled Viscoelastic Surfactant Micelles with pH-Responsive Behavior: A New Fracturing-Displacement Integrated Working Fluid for Unconventional Reservoirs

Xiaochen Li,* Xianbin Zhang, Leilei Wang, Fei Wen, Yurong Chen, Qichao Lv, Hong Ma, Anliang Chen, Ruxue Wang, Leixu Chen, Qian Wang, Dianbin Dong, Shaoying Xu, and Qiqi Niu*

Cite This: *ACS Omega* 2024, 9, 22691−22702

Read Online

ACCESS | Metrics & More | Article Recommendations

ABSTRACT: The integrated fracturing and oil recovery strategy is a new paradigm for achieving sustainable and cost-effective development of unconventional reservoirs. However, a single type of working fluid cannot simultaneously meet the different needs of fracturing and oil displacement processes. Here, we develop a pH-responsive fracturing-displacement integrated working fluid based on the self-assembled micelles of N,N-dimethyl oleoamine propylamine (DOAPA) and succinic acid (SA). By adjusting the pH of the working fluid, the DOAPA and SA molecules can be switched repeatedly between highly viscoelastic wormlike micelles and aqueous low-viscosity spherical micelles. The zero-shear viscosity of the working fluid enriched the wormlike micelles can reach more than 93,100 mPa·s, showing excellent viscoelasticity and sand-carrying properties. The working fluid is easy to gel-break when it encounters oil, generating a low-viscosity liquid without residue. In addition, the system has strong interfacial activity, which can greatly reduce the oil−water interfacial tension to form emulsions and can achieve reversible demulsification and re-emulsification by adjusting pH. Through the designed and fabricated microfluidic chip, it can be visualized that under the synergistic effect of viscoelasticity and interfacial activity DOAPA/SA can effectively expand the swept volume of tight fractured formations, promote pore wetting reversal and crude oil emulsification, and improve the displacement efficiency. The DOAPA/SA meets the design requirements of the fracturing-displacement integrated working fluids and provides a novel method and idea for constructing the integrated working fluids suitable for fracturing and displacement in unconventional reservoirs.

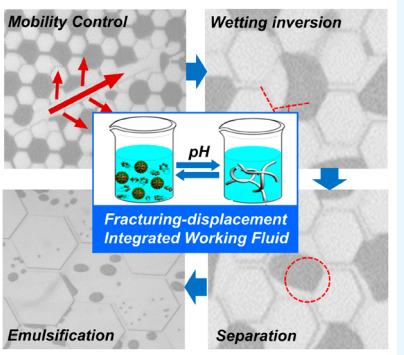

1. INTRODUCTION

Over the past five years, unconventional reservoirs have become a pivotal force in the development of oil and gas resources.[1,2] However, the sustainable and cost-effective development of unconventional reservoirs has been a great challenge.[3,4] Hydraulic fracturing technology is a commonly utilized method of stimulating unconventional reservoir development.[5−7] Hydraulic fracturing not only facilitates the increase of production in the area from which the well is extracted but also effectively modifies the reservoir characteristics to connect the low-permeability reservoir to the wellbore, expanding the area of wellbore mobilization, thus increasing the recovery of the resources.[8] This process involves injecting a significant volume of high-viscosity liquid into the well to induce fractures within the formation. To maintain the formation's high conductivity, proppant is also injected to support these fractures.[9] However, due to the limitations of unconventional reservoir pore characteristics, formation clay water sensitivity and other factors, the suitable fracturing fluid system needs to meet the requirements of high viscosity, high viscoelasticity, and shear resistance of the traditional system and also needs to have excellent breakage and low residual properties for minimizing the damage of the fracturing fluid to the reservoir.

In existing water-based fracturing fluids, five types of materials, guar gum, cellulose, xanthan gum, polyacrylamide and their derivatives, are usually added to the fracturing fluid to increase the viscoelasticity of the system and reduce frictional resistance guar gum.[5,10−12] Although these additives effectively enhance the fracturing fluid's ability to create fractures, they are highly susceptible to the generation of insoluble residues that cannot be ablated within a short period, resulting in blockage and damage to reservoir pores.[13,14] In addition, fractures produced by such fracturing fluids tend to propagate centrally at longitudinal heights, whereas the main objective when treating low-permeability areas with poor filtration

Received: January 14, 2024
Revised: April 17, 2024
Accepted: April 22, 2024
Published: May 14, 2024

properties is to form a transversely induced fracture as deep as possible into the producing formation.[10,12,15,16] It exposes the fatal shortcoming of traditional water-based fracturing fluids in their inability to balance reservoir modification and reservoir damage when confronted with unconventional reservoirs.

To solve the problem of traditional water-based fracturing fluids, researchers constructed a viscoelastic fracturing fluid system based on the principle of self-assembly of surfactant molecules to form wormlike micelles.[17,18] This self-assembly process relies on the intermolecular hydrophobic forces of surfactants, which allow the molecules to build up in an aqueous environment with long hydrophobic chains facing inward and hydrophilic groups facing outward in a directional manner, resulting in the formation of a wormlike micellar structure when the concentration reaches a critical value. Therefore, the fracturing fluid system can easily break the micelles and form a low-viscosity residue when it contacts the crude oil or other hydrocarbons in the formation, thus greatly reducing damage to the reservoir pore space.[19−21] This is why viscoelastic fracturing fluids are also known as clean fracturing fluids.

However, a large amount of surfactant needs to be added during the preparation and maintenance of the viscoelastic fracturing fluid system to ensure that the concentration of surfactant molecules in the system is much higher than the critical micelle concentration to form wormlike micelles. Published research information on the surfactants market by Precedence research, Allied market research, and Markets and Markets shows that the global surfactants market is expected to grow to a value of more than USD 80 billion by 2030.[8] As a result, the high cost during periods of low to medium crude oil prices limits the widespread use of this system in unconventional reservoirs. In the face of this dilemma, researchers have added appropriate amounts of nanoparticles, guar gum, cellulose, polymer, etc. to the viscoelastic fracturing fluid system to minimize the cost pressure brought by surfactants.[17,22−24] However, for complex formations, the addition of traditional fracturing fluids to low-damage viscoelastic fracturing not only has limited space for cost reduction but also cannot effectively avoid the problem of reservoir damage.

In recent years, researchers have increased the packing density of surfactant molecules by growing the hydrophobic long chains of surfactants,[18,25] or constructing gemini or trimeric surfactants with multiple hydrophobic chains to achieve viscoelastic effects at low concentrations.[26−28] However, the high cost caused by the complicated synthesis method and low yield has hindered the marketization of the products. Consequently, reducing reservoir damage and improving economic efficiency remain crucial hurdles for the sustainable development of unconventional reservoirs.[29,30] Fortunately, the huge reserves and development potential of unconventional reservoirs have always inspired petroleum engineers and researchers. In recent years, researchers have proposed the integrated technology of fracturing and oil recovery, which can simultaneously achieve reservoir stimulation and enhanced oil recovery.[31−33] Integrated technology can effectively reduce production processes, reduce mining costs, and improve economic benefits. Although there have been some reports of preliminary exploration of this technology, these reported cases are still weak compared to the urgent need for unconventional oil and gas reservoir development.

Here, based on the concept of an integrated working fluid, we have constructed a pseudogemini surfactant structure with pH responsiveness by compounding commercial surfactant DOAPA and dicarboxylic SA molecule, which can independently form a fracturing-displacement integrated working fluid with excellent viscoelastic properties and interfacial activity. Then, the rheological properties, pH response cyclicity, and microstructure of the system were characterized, and the fracturing performance, emulsification performance, oil displacement, and imbibition capacity of the system were systematically studied. The excellent DOAPA/SA can provide a reference for the integrated technology scheme of fracturing and oil recovery in unconventional reservoirs, which has a positive significance for improving the economic and efficient development of unconventional reservoirs.

2. EXPERIMENTAL SECTION

2.1. Materials. Succinic acid (SA), sodium hydroxide (NaOH), and hydrochloric acid (HCl, 37%) were procured from Shanghai Macklin Biochemical Co. Ltd. N, N-dimethyl oleoamine propylamine (DOAPA) was obtained from Shanghai Yincong New Material Technology Co. Ltd. The proppant used in the study was graciously provided by Shengli Oilfield, China. This proppant was characterized by being a spherical ceramsite with a diameter ranging from 380 to 425 μm. Deionized water with an electrical resistivity of 18.0 MΩ cm was utilized for all measurements. Figure 1 showcases the molecular structure formulas of both DOAPA and SA.

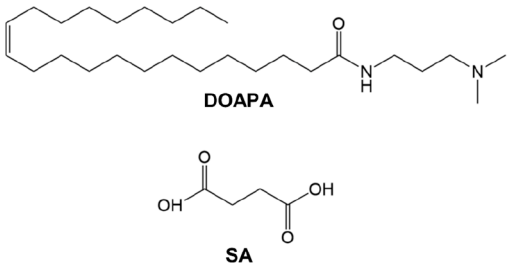

Figure 1. Molecular structural formulas of DOAPA and SA.

2.2. Sample Preparation. Specific quantities of DOAPA and SA were dissolved in deionized water and blended using mechanical stirring. Subsequently, aqueous solutions of HCl or NaOH were introduced into the mixture to attain the desired pH level. The prepared samples were then stored at room temperature for a minimum of 1 day before commencing subsequent measurement experiments. In subsequent testing and evaluation sessions for fracturing, emulsification, oil displacement, and imbibition, a concentration of 240 mM DOAPA+120 mM SA is consistently used if the solution concentration is not explicitly stated.

2.3. Rheology. The HAAKE RS6000 rheometer equipped with a sealable coaxial cylindrical sensor system (Z41 Ti) was utilized to measure the rheological properties of the prepared samples. During viscosity determination, the shear rate was set within the range of 0.01−1000 s^{-1}, and an appropriate test duration was selected. The zero-shear viscosity of the sample was extrapolated from the first Newtonian plateau value observed at low shear rates. For viscoelasticity tests, the sample was initially subjected to a fixed frequency of 1.0 Hz to identify the linear viscoelastic zone, followed by a frequency sweep conducted at an appropriate stress level. The temperature

https://doi.org/10.1021/acsomega.4c00459
ACS Omega 2024, 9, 22691−22702

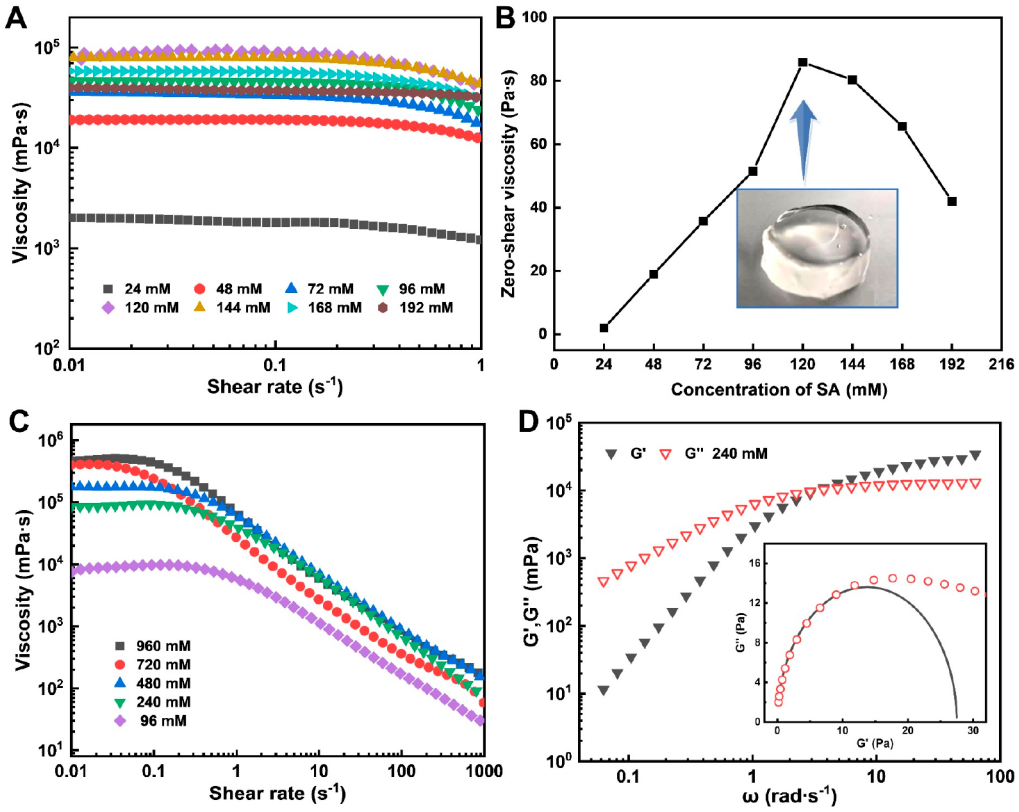

Figure 2. (A) Steady shear rheology and (B) zero-shear viscosity of DOAPA/SA at different SA concentrations. (C) Steady shear rheology with different concentrations of DOAPA/SA. (D) Frequency sweep rheology and Cole−Cole diagram of DOAPA/SA.

regulation was achieved using a cyclic water bath, with the test temperature set at 25 °C, unless otherwise specified.

2.4. Cryogenic-Transmission Electron Microscopy (Cryo-TEM). To observe the microstructures of the samples, a JEM-1400 Plus TEM instrument operating at 120 kV was utilized. Approximately 5 μL of the sample was applied onto a copper mesh and evenly spread across its surface. It was crucial to ensure that the thickness of the sample layer was sufficiently thin, as thicker layers could not be frozen into a glassy state. Subsequently, the prepared sample on the copper mesh was immersed in liquid ethane. Afterward, the precooled sample was carefully transferred to a transmission electron microscope using a sample rod, while maintaining a controlled temperature of −174 °C throughout the observation process.

2.5. Fracturing Fluid Performance. The DOAPA/SA was prepared using the mechanical stirring method and subsequently uniformly mixed with the proppant. The concentration of the proppants in the fluid carrying them was set at 0.02 g·cm^{-3}. To measure the settling velocities of the proppants, a cuboid colorimeter cell with dimensions of 90 mm in height and 6 mm in thickness was employed. A water bath was utilized to regulate the temperature inside the colorimeter cell. Injection of the proppant-carrying fluid into the cell allowed for monitoring of the proppants using a digital camera (VHX-5000, Keyence, Japan), which was equipped with a portable 3D scanner capable of capturing a large depth-of-view. A specific amount of kerosene was added to the fracturing fluid and stirred for 5 min. Subsequently, the apparent viscosity of the sample was continuously measured using HAAKE RS6000 rheometer at a temperature of 80 °C. The time taken for the sample's apparent viscosity to decrease below 5.0 mPa·s was defined as the breaking time, and the apparent viscosity at this point represented the viscosity of the gel-broken fluid.[34]

2.6. Emulsifying Capacity. Microscopic morphology of the gel-broken fluid was observed using an Olympus optical microscope. The oil−water emulsion was prepared by homogenizing 5.0 mL of deionized water and 5.0 mL of kerosene at room temperature using high-speed homogenization. The water phase contained a surfactant solution with varying concentrations of SA and DOAPA, with a constant SA to DOAPA ratio of 1:2. The oil−water interfacial tension was measured using a Dataphysics SVT20N interfacial tensiometer. The experiments were conducted at a temperature of 25 °C, a rotational speed of 6000 rpm, and a duration of 6000 s.

2.7. Oil Displacement Measurement. To investigate the oil displacement effect of the integrated working fluid in the porous medium of a low-permeability unconventional reservoir, a microfluidic chip was designed and fabricated using photochemically etched glass substrates. The pore throat of the porous medium is designed as a regular shape, and the pore throat is a square hexagon of equal size, which is connected to the neighboring pore throats through a narrow channel at the apex of the hexagon. The porous medium of the microfluidic chip has an area of 50 × 50 mm, the width of the pore throat is 50−60 μm, and the size of the narrow channel is 8−12 μm. To simulate the development of cracks in the formation, randomly distributed rectangular channel cracks with widths of 50−100 μm were set up. Before the experiments, the porous medium was evacuated and filled with water. Then, oil was injected into the micromodel to saturate it until no water flowed out. For the experiment, the chip was placed horizontally, the working fluid was injected from the left inlet, and the output fluid flowed out from the

https://doi.org/10.1021/acsomega.4c00459
ACS Omega 2024, 9, 22691−22702

right outlet. The injection rate was 0.01 mL·min^{-1} and the injection volume was calculated as pore volume (PV). A high-resolution microscope was used to record microscopic images and observe the flow behavior of the fluid in the porous medium.

2.8. Imbibition Capacity Measurement. The volumetric method was chosen for the imbibition experiment, and the imbibition capacity was evaluated by calculating the degree of extraction. The dried natural cores (Φ 0.3 × 90 mm) were placed on an electronic balance to be weighed and recorded, then vacuumed and saturated with oil for 7 days, the cores were extracted and weighed after removing the surface oil, and the original oil-containing volume of the cores was calculated. The core was placed in an imbibition bottle and the integrated working fluid was slowly injected into the glass tube scale. Observe the oil production on the surface of the core and read and record the volume of oil produced by suction according to the change in the height of the liquid level. When the reading of the imbibition bottles no longer changes, shake the bottle to detach the oil droplets from the core surface, and after stabilization, the reading is the final volume of crude oil extracted through the action of imbibition. The final volume of oil produced as a percentage of the saturated oil volume is the degree of recovery by imbibition effect.

3. RESULTS AND DISCUSSION

3.1. Rheological Properties of the DOAPA/SA System. The effect of SA concentration on the maximum zero-shear viscosity of the DOAPA/SA system was first investigated. The DOAPA concentration in the aqueous solution was maintained at 240 mM, and the system's pH was adjusted using HCl and NaOH. Preliminary experimental results demonstrated that the zero-shear viscosity of the DOAPA/SA system peaked at pH 7.56. Figure 2A and 2B depicts the steady shear curves and corresponding zero-shear viscosity of the DOAPA/SA system at various SA concentrations at a temperature of 25 °C. The maximum zero-shear viscosity of the system exhibited an upward trend with increasing SA concentration when the SA was below 120 mM. When the concentration of SA increased to 120 mM, the molar ratio of DOAPA to SA was 2:1, and the solution formed a self-supporting gel with a maximum zero-shear viscosity of about 93,100 mPa·s (Figure 2B).

Furthermore, various sample systems were prepared with different concentrations of DOAPA by maintaining a fixed molar ratio of DOAPA to SA at 2:1. The steady rheological properties and corresponding zero-shear viscosity of these systems were investigated at pH 7.56, and the results are displayed in Figure 2C. The zero-shear viscosity of the system increased as the concentration of DOAPA in the aqueous solution increased. In addition, it can be seen from Figure 2C that when the DOAPA concentration exceeds 240 mM, especially 720 mM and 960 mM, there is no significant difference in the viscosity of the system at high shear rates. Therefore, taking into consideration the thickening performance and economic cost of fracturing fluid application, the optimal concentration of DOAPA was determined to be 240 mM, with a corresponding DOAPA/SA formula of 240 mM DOAPA+120 mM SA.

A common feature of the five DOAPA/SA solutions of different concentrations in Figure 2C is that stable shear rheological measurements appear as a Newtonian plateau within the shear-rate range from 0.01 to 0.3 s^{-1}, accompanied by shear thinning over a critical shear rate. Such a shear-thinning behavior of surfactant solutions is normally evidence for the existence of wormlike micelles. The rheological characteristics of the viscoelastic micelle system at the oscillatory shear frequency (ω) follow the Maxwell fluid behavior with single stress relaxation time (τ_R), and the elastic modulus (G') and viscous modulus (G'') are related to the ω as follows[35]

$$G'(\omega) = \frac{(\omega\tau_R)^2}{1 + (\omega\tau_R)^2} G_0 \quad (1)$$

$$G''(\omega) = \frac{\omega\tau_R}{1 + (\omega\tau_R)^2} G_0 \quad (2)$$

At high ω, G' usually reaches an extreme value, which is known as the plateau modulus, i.e., G_0. According to the above equation, the relaxation time τ_R at the intersection of G' and G'' curves can be estimated by the reciprocal of the critical frequency.

Figure 2D illustrates the variation curves of the G' and G'' of the DOAPA/SA with ω. At a pH of 7.56, the viscous modulus surpasses the elastic modulus at low shear frequencies, while the elastic modulus overtakes the viscous modulus at high shear frequency ranges. These findings indicate a gradual transition of the solution from a viscous fluid to an elastic fluid as the shear frequency increases at pH 7.56, lending support to the presence of wormlike micelles within the DOAPA/SA solution.[36,37] The dynamic viscoelasticity of the wormlike micelles system conforms to the Maxwell model, and its Cole−Cole diagram is presented as a semicircle with a diameter equal to G_0 in the low shear frequency range.[38] Figure 2D demonstrates the Cole−Cole diagram of the DOAPA/SA at pH 7.56, with the black line representing the fitting of experimental values according to the Maxwell model. The rheological behavior of the DOAPA/SA aligns well with the Maxwell model at low shear frequencies but deviates from the semicircular curve at high shear frequencies. This phenomenon can be attributed to the rouse and breathing effect of wormlike micelles, which undergo continuous breakage and reorganization during the shearing process.[39] Consequently, despite the inconsistent adherence of experimental values to the Cole−Cole semicircle model at high frequencies, the results still confirm the formation of wormlike micelles within the DOAPA/SA at pH 7.56. Therefore, the increase in solution zero-shear viscosity in Figure 2C can be attributed to the higher DOAPA concentration leading to an increased likelihood of molecular self-assembly into wormlike micelles, as well as a greater degree of overlap and entanglement between micelles. However, when the DOAPA concentration exceeds 720 mM, the branching of wormlike micelles curtails the rising trend of system viscosity.

In addition, the unique 2:1 ratio between the two substances DOAPA and SA is particularly interesting. According to theory, two DOAPA molecules can form a pseudogemini surfactant molecular structure by being bound to oppositely charged SA molecules via electrostatic attraction.[40] Additionally, the dispersed aggregation state of surfactant molecules is typically described by the critical packing parameter *CPP* ($CPP = V/a_0l_c$). Here, V represents the volume of the hydrophobic tail chain, a_0 denotes the minimum cross-sectional area of the hydrophilic head groups, and lc signifies the length of the hydrophobic chain.[36] A *CPP* value between 1/3 and 1/2 is favorable for the formation of wormlike micelles.[36] In

https://doi.org/10.1021/acsomega.4c00459
ACS Omega 2024, 9, 22691−22702

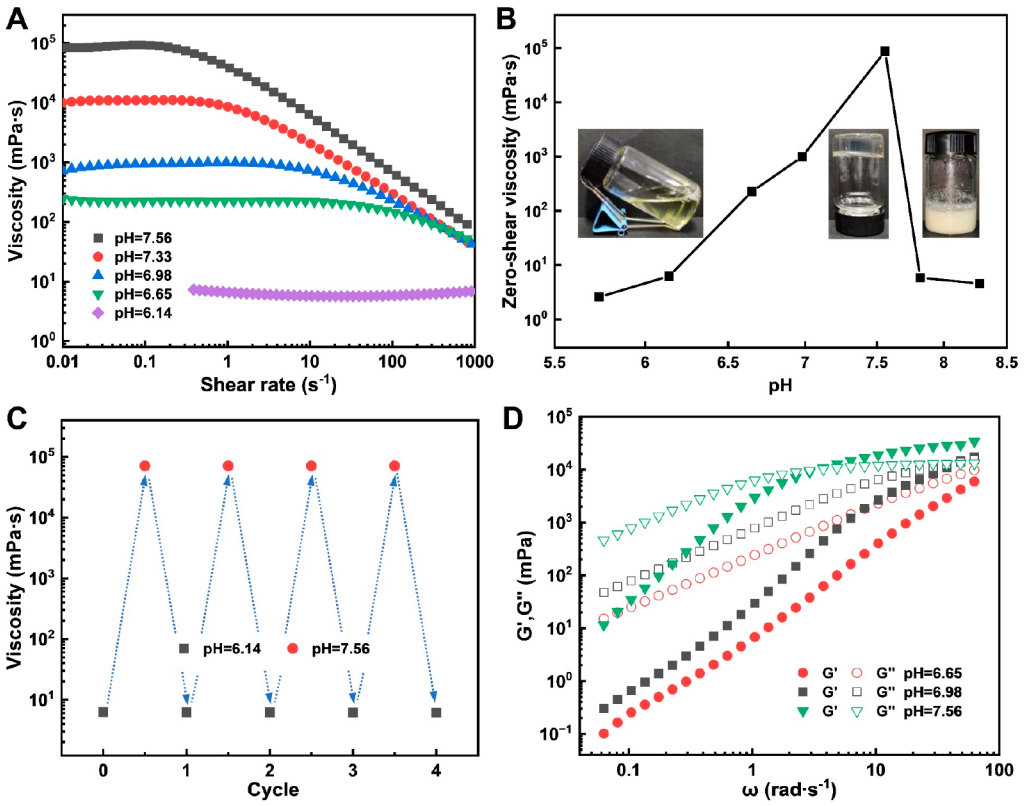

Figure 3. (A) Steady shear rheology and (B) zero-shear viscosity of the DOAPA/SA with different pH. (C) Variation of zero shear viscosity with the number of cycles by changing pH. (D) Frequency sweep rheology of DOAPA/SA with different pH.

comparison, the a_0 of the pseudogemini surfactant molecular structure is significantly smaller than that of a single long-chain surfactant molecule because the hydrophilic headgroups are bridged by small SA molecules.[41] The bridging effect reduces the electrostatic repulsion between surfactant head groups, bringing the hydrophilic head groups of the molecules closer together.[42] The bridged pseudogemini surfactant has two hydrophobic long chains, with a volume of the hydrophobic tail chain twice that of a single surfactant.[41] Consequently, the *CPP* of the pseudogemini surfactant readily falls within the favorable range of 1/2−1/3, promoting the formation of highly viscoelastic wormlike micelles.[40] On a macroscopic level, a pseudogemini surfactant structure forms between the molecules and self-assembles into wormlike micelles when the molar ratio of DOAPA to SA is 2:1.[36]

3.2. pH Responsiveness of the DOAPA/SA. The steady shear curves of the DOAPA/SA at different pH levels are presented in Figure 3A. The concentrations of DOAPA and SA are 240 mM and 120 mM, respectively. At a pH of 6.14, the solution demonstrates a viscosity of approximately 6.50 mPa·s, which remains constant irrespective of the increasing shear rate, indicating its Newtonian fluid behavior. Within the pH range of 6.65−7.56, the solution exhibits a consistent viscosity at low shear rates while displaying shear-thinning behavior at high shear rates. Figure 3B illustrates the appearance and zero-shear viscosity of DOAPA/SA for various pH levels. It demonstrates that the prepared DOAPA/SA displayed a transparent aqueous fluid appearance with an initial pH of 5.74 and a zero-shear viscosity of 2.58 mPa·s. Subsequently, the system's zero-shear viscosity exhibited a significant increase as the pH elevated. At pH values of 6.65 and 6.98, the zero-shear viscosity reached 226.7 mPa·s and 988.5 mPa·s, respectively, accompanied by the DOAPA/SA gradually sliding toward the wall within seconds of inversion. Increasing the pH to 7.56 resulted in the solution's zero-shear viscosity attaining a maximum value of approximately 93,100 mPa·s, accompanied by the solution exhibiting a transparent gel state and a lack of flow. Nevertheless, further increases in pH caused a sharp decrease in the system's zero-shear viscosity. As the pH rose from 7.56 to 7.82, the zero-shear viscosity once again diminished, reaching 5.84 mPa·s, while the initial clarified appearance of the DOAPA/SA transformed into a turbid state. The intermolecular interactions and micelle types within the DOAPA/SA system are influenced by the ionization degree of DOAPA and SA, resulting in corresponding changes in the appearance and viscosity of the fluid, thus exhibiting pH responsiveness.

To investigate the cyclic reversibility of the pH response behavior of the DOAPA/SA, we examined the changes in zero-shear viscosity by repeatedly adjusting the pH between 6.14 and 7.56 at a temperature of 25 °C. The results are presented in Figure 3C. At a pH of 6.14, the zero-shear viscosity of the fracturing fluid was approximately 6.5 mPa·s. Upon adjusting the pH from 6.14 to 7.56, there was a significant increase in the zero-shear viscosity to approximately 90,800 mPa·s, representing an increase of 5 orders of magnitude. Subsequently, when the pH was decreased back to 6.14, the zero-shear viscosity dropped to approximately 6.0 mPa·s. This pH-responsive behavior, whereby viscosity changes with the pH of the system, can be cycled more than four times within a specific pH range. These findings demonstrate that the DOAPA/SA developed in this study exhibits excellent pH reversible switchability, enabling it to transition between a viscoelastic solution and a low-viscosity fluid within a narrow pH range. It is important to

https://doi.org/10.1021/acsomega.4c00459
ACS Omega 2024, 9, 22691−22702

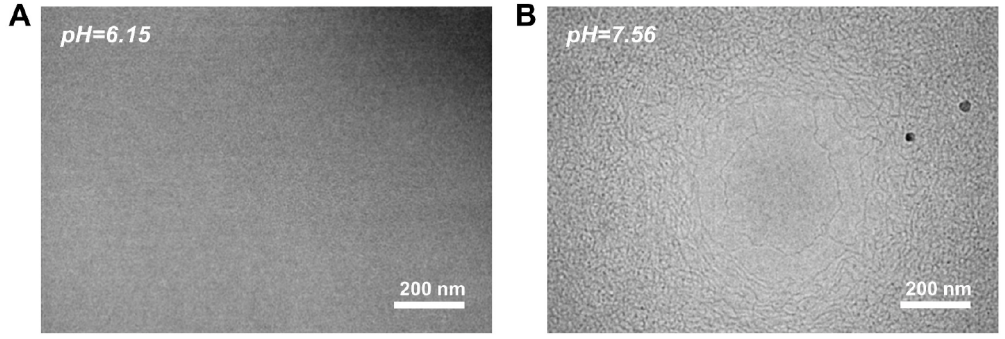

Figure 4. (A) Cryo-TEM micrograph of DOAPA/SA solution at pH 6.15 and (B) at pH 7.56.

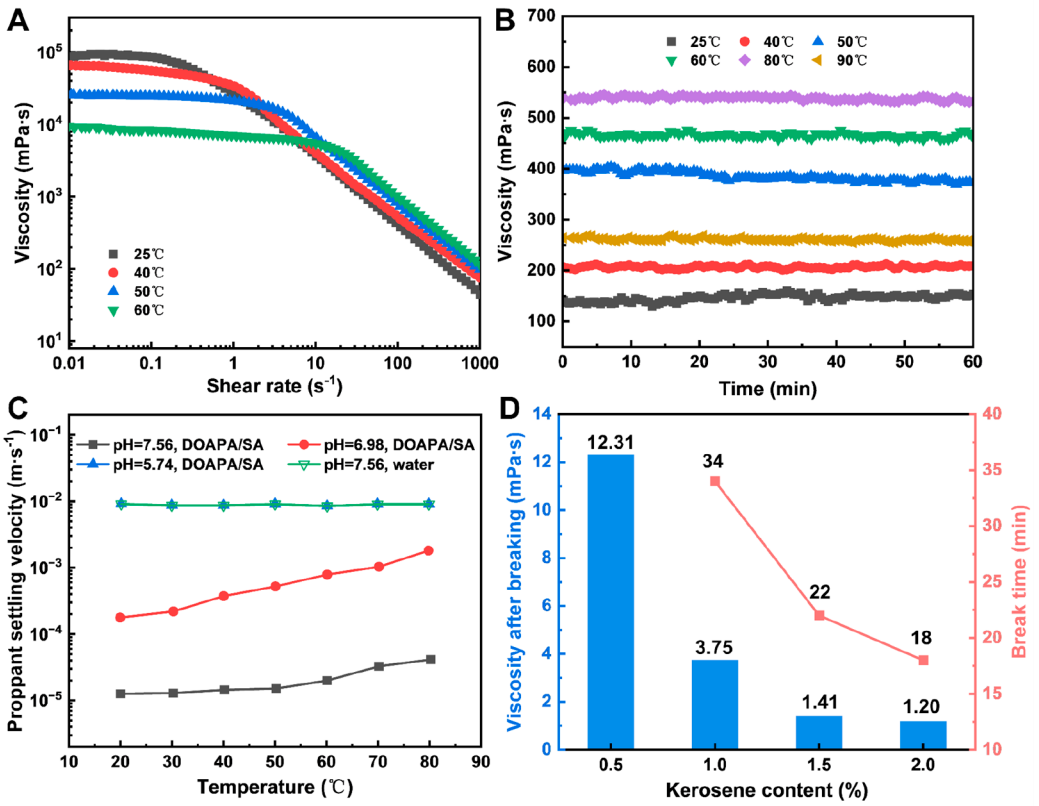

Figure 5. (A) Steady shear viscosity plots of DOAPA/SA with different temperatures. (B) Viscosity variation curves of DOAPA/SA with shear time. (C) Variation of proppant settling velocity with temperature. (D) Breaking time and viscosity of fracturing fluid vary with kerosene content.

note that the addition of salt to a wormlike micelles system can alter its rheological properties due to changes in micellar topology.[43,44] Typically, the viscosity of a wormlike micelles system increases up to a critical value as the salt concentration rises.[45] Beyond the viscosity peak, further increases in salt concentration led to a drop in viscosity. In our study, the surfactant concentration is high, and the salt concentration only increases within a small range during the four cycles of reversible pH regulation. Therefore, the salt produced as a result of acid/base regulation has no significant impact on the viscosity of the system.

Figure 3D gives the G' and G'' of the DOAPA/SA at different pH values. The results show that within the tested shear frequency range, the viscous modulus of the DOAPA/SA is higher than the elastic modulus and exhibits viscous behavior when the pH ranges from 6.65 to 6.98. Moreover, the plateau modulus G_0 of the DOAPA/SA solution increased significantly with pH from 6.65 to 7.56, reflecting a change in the molecular aggregation structure in the system, which was mainly reflected in the increase in the entanglement density. Meanwhile, along with the increase of pH in the DOAPA/SA solution, the frequency ω_c at the intersection of G' and G''i is shifted to a higher ω, which corresponds to a faster relaxation process and a shorter relaxation time τ_R. In Figure 3D, the viscoelastic modulus of the system does not intersect in the ω test range when the system pH is 6.65. At a system pH of 6.98, the relaxation time τ_R is about 0.023 s, whereas the system pH became 7.56 and the relaxation time τ_R is elevated to 0.30 s accordingly. The large extension of the relaxation time is a visual reflection of the growth of molecular aggregation micelles in solution, or changes in the structure of the aggregates.[46,47] For example, from small, simple spherical micelles to larger, intertwined wormlike micelles, or more complex vesicles and other structures.

https://doi.org/10.1021/acsomega.4c00459
ACS Omega 2024, 9, 22691−22702

To observe the microstructures of micelles in a 240 mM DOAPA/120 mM SA solution at various pH levels, cryo-TEM was employed. As depicted in Figure 4A and 4B, a significant change in the micelle microstructure is observed as the pH increases from 6.15 to 7.56. At pH 6.15, no wormlike micelles were present in the DOAPA/SA system, and the solution displayed a low-viscosity Newtonian fluid behavior. Conversely, at pH 7.56, the DOAPA/SA system demonstrates densely packed wormlike micelles that intertwined to form a larger network structure. Hence, the reversible switch ability of the rheological properties of the DOAPA/SA solution can be fundamentally attributed to the transformation of micelle types within the system based on pH. Based on the alterations in the microscopic molecular structure of the DOAPA/SA solution and the viscoelastic properties of the macro solution, it can be anticipated that the molecular integration of DOAPA and SA is highly suitable for meeting the performance criteria of a viscoelastic fracturing fluid.

3.3. DOAPA/SA Fracturing Fluids Performance. The steady shear curves of the DOAPA/SA at various temperatures are presented in Figure 5A. In the DOAPA/SA system, the viscosity curves exhibit a plateau value at low shear rates, known as zero-shear viscosity. As the temperature increased, the zero-shear viscosity gradually decreased, reaching approximately 9280 mPa·s at 60 °C. Similar observations have been reported in other wormlike micelle systems, which are typically sensitive to ambient temperature.[34,48] Typically, a 1 order of magnitude decrease in zero-shear viscosity occurs with every 10 °C increase in temperature.[49,50] However, for the DOAPA/SA, the zero-shear viscosity only decreased by 1 order of magnitude when the temperature was raised from 40 to 60 °C, indicating an improvement in temperature resistance compared to conventional clean fracturing fluids.

However, it is not enough to discuss the temperature resistance of DOAPA/SA systems in the lower shear range or at rest. The working fluid is always flowing during the fracturing process or oil drive, so the focus should be on the effect of temperature on the viscosity of the system in the higher shear range behind the Newtonian platform. It is worth mentioning that in Figure 5A, the increase in temperature causes the Newtonian plateau of the stable shear curve to extend. After the critical shear rate, the viscosity curve of the system under higher shear decreases with the increase of temperature, showing a regular step pattern. It is shown that the shear viscosity of the system increases with the increase of temperature in the range of high shear rate. This indicates that the DOAPA/SA system has excellent thermal stability at high shear. For conventional fracturing fluid systems, the effect of temperature on viscosity has been negative, both at static and under shear. For the DOAPA/SA system, however, the effects of temperature appear to be contradictory but are not. This process is not difficult to understand, in the stationary state or low shear conditions, the increase in temperature will promote the thermal movement of molecules in the system, the microscopic part of the worm-like micelle structure disintegration, the entanglement between the micelle loose. Therefore, the macroscopic performance of zero shear viscosity that is the overall decline of the Newtonian platform. Under high shear, the one-dimensional linear wormlike micelles are more tightly entangled with each other, which can better resist the negative effects of the intensified molecular thermal movement. In addition, the shear will cause the wormlike micelles to continuously change from disintegration to reconstruction, and the macroscopic temperature resistance of the system is shown to be enhanced under high shear.[37,38]

Figure 5B depicts the viscosity variation curves with shear time at different temperatures, with a fixed shear rate of 170 s^{-1}. In the temperature range of 25−80 °C, the stabilized viscosity of DOAPA/SA increases gradually with the increase of temperature, from 167.5 mPa·s at 25 °C to 549.1 mPa·s at 80 °C. At 90 °C, the viscosity of DOAPA/SA decreases significantly, but the lowest value of shear viscosity remains above 254.0 mPa·s. This indicates that some of the wormlike micelles in the system are destroyed and the network structure is disintegrated at this temperature, but there is still a sufficient amount of wormlike micelle structure to guarantee the viscosity of the system. According to the Petroleum Industry Standard of the People's Republic of China SY/T 5107−2005, the tolerance temperature of fracturing fluids is defined as the temperature at which the apparent viscosity reaches 50 mPa·s under a shear rate of 170 s^{-1}. Therefore, based on this criterion, the DOAPA/SA developed in this study is suitable for medium and low-temperature reservoirs.

Proppant-carrying ability is a crucial characteristic of fracturing fluid, as it determines the ability of the fluid to transport proppant particles from the vicinity of the wellbore to distant areas and from the main fracture to smaller fractures. To assess the proppant-carrying ability, a static settlement test was conducted using different fluids. As depicted in Figure 5C, both water with a pH of 7.56 and a DOAPA/SA with a pH of 5.74 exhibited a similar proppant settling rate of approximately 9×10^{-3} m·s^{-1}, which indicates a poor or unacceptable velocity (vs >8.3×10^{-4} m·s^{-1}) for proppant settling.[51] The presence of a wormlike micelle structure enhanced the fluid's proppant-carrying ability. Figure 5C illustrates that the proppant settling velocity in the DOAPA/SA with a pH of 6.98 is one magnitude lower than that in both water with a pH of 7.56 and the DOAPA/SA. This can be attributed to the support provided by the viscous wormlike micelle structure, preventing the proppant from sinking until the structure deforms or ruptures. However, even in the DOAPA/SA with a pH of 6.98, the desired proppant settling velocity (vs <8.3×10^{-5} m·s^{-1}) was not achieved.[51] Figure 5C further reveals that the proppant settling velocity in the DOAPA/SA (pH = 7.56) was one magnitude lower than that in the DOAPA/SA (pH = 5.74), across temperatures ranging from 20 to 80 °C. Hence, the DOAPA/SA at pH = 7.56 showcases excellent proppant-carrying ability.

The solubilization of hydrocarbons into the hydrophobic core of micelles can impact the distribution of surface charge in wormlike micelles, causing a transition from wormlike to spherical micelles.[52] Consequently, this transition leads to a loss of viscoelasticity. To evaluate the effectiveness of the DOAPA/SA in breaking gels, kerosene was employed as a surrogate for the formation of hydrocarbon. Specifically, the viscosity and gel-breaking time of the resulting fluid were measured at 80 °C. Figure 5D presents the data, indicating that both the gel-breaking time and viscosity decreased as the volume of kerosene increased. For instance, when the kerosene volume reached 1.0%, the viscosities of the gel-broken fluid were below 5.0 mPa·s within an hour. Controlling the gel-breaking time of the DOAPA/SA can be achieved by adjusting the amount of the kerosene breaker. Observations of the gel-broken fluids reveals their clarity and absence of residues. Nonetheless, even after collapse, surfactant molecules can still migrate deeper into the formation due to pressure, coming into

https://doi.org/10.1021/acsomega.4c00459
ACS Omega 2024, 9, 22691−22702

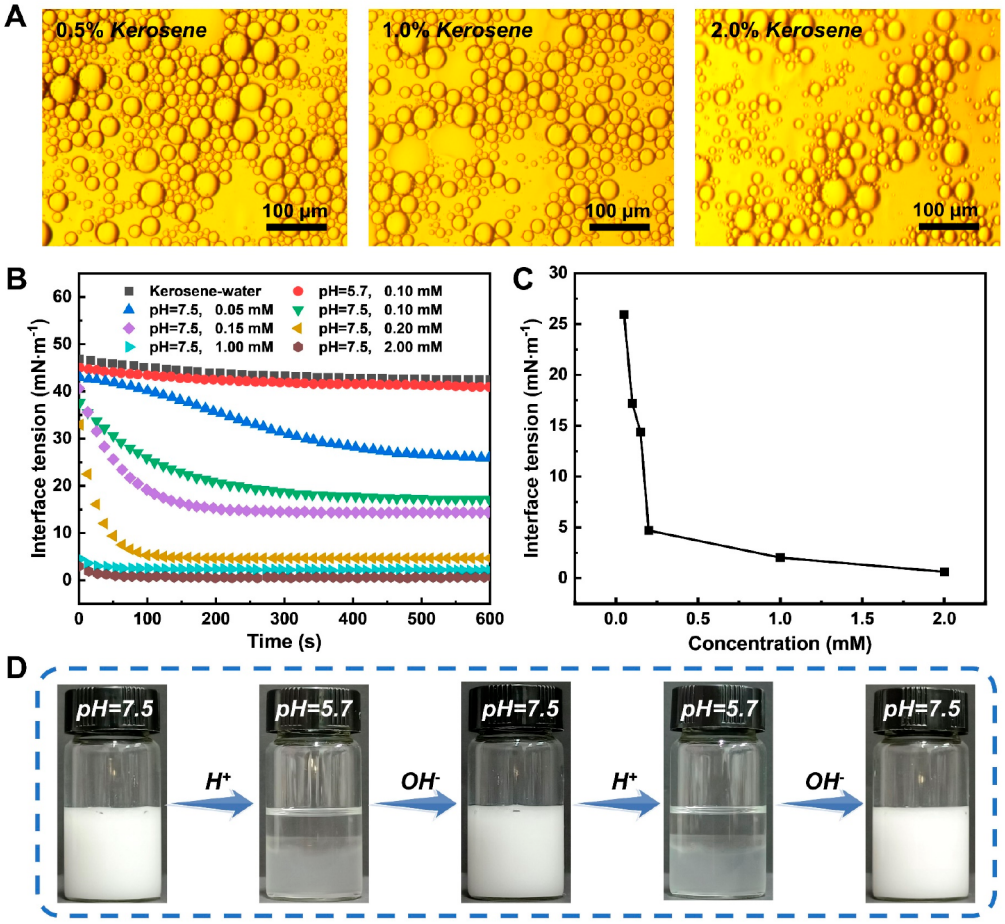

Figure 6. (A) Optical microscopic images of gel-broken fluids. (B) Interfacial tension of DOAPA/SA at different pH values. (C) Interfacial tension of DOAPA/SA at different concentrations. (D) O/W emulsion appears at different pH values.

contact with rock and crude oil. As can be imagined, DOAPA/SA surfactants are not only an essential component in the construction of wormlike micelles, but also an effective component in reducing oil−water interfacial tension, promoting oil droplet emulsification in the reservoir, and thus enhancing oil recovery.

3.4. DOAPA/SA Emulsifying Performance. Fracturing and oil displacement fluids for unconventional oil and gas exploration and development should not only meet the requirements of the fracturing process but also have the function of emulsification and oil displacement. Optical microscope images of DOAPA/SA after gel breaking with different contents of kerosene are shown in Figure 6A. From the optical images, it can be seen that kerosene mixed with DOAPA/SA formed an oil-in-water emulsion, which proves that the DOAPA/SA system has the emulsifying ability after breaking the glue.

The emulsion system was further explored by an interfacial tensiometer (Figure 6B). The interface tension measurements show that the oil−water interfacial tension decreased from 42.50 mN·m^{-1} to 25.93 mN·m^{-1} in the kerosene-water system containing 0.05 mM DOAPA/SA. With the increase of DOAPA/SA concentration in the emulsion system, the oil−water interfacial tension decreases continuously, and the equilibrium time of the oil−water interfacial tension is also shortened simultaneously. At a DOAPA/SA concentration of 2.0 mM, the interfacial tension of kerosene-water is reduced to 0.62 mN·m^{-1}, and the equilibrium time was only 52 s. This further demonstrates the excellent interfacial activity of DOAPA/SA at low concentrations. From Figure 6C, it can be seen that the interface tension of kerosene-water decreases sharply at the initial stage with the increase of surfactant DOAPA/SA concentration. The oil−water interface tension is reduced at a slower rate when the surfactant concentration exceeds about 0.2 mM, which can be determined to be close to the critical micelle concentration of the DOAPA/SA combination. The critical micelle concentration of 0.2 mM is negligible compared to the 240 mM DOAPA/SA fracturing fluid system. These results indicate that the DOAPA/SA combination will still have good interfacial activity even after deeper penetration into the formation and gradual reduction of the fluid concentration by rock adsorption and laminar separation. This process of concentration reduction facilitates the transition from a highly viscoelastic fracturing fluid system to a high interfacial activity-repellent system.

In addition, we examined the effect of pH on DOAPA/SA interfacial activity during interface tension measurements. As shown in Figure 6B, the interfacial tension curves of kerosene and water coincide with the initial state when the aqueous solution pH = 5.7. This reflects the significant effect of pH on the interfacial tension of kerosene-water mixtures containing DOAPA/SA. Figure 6C and 6D present the appearance and optical micrographs of the O/W emulsion. The O/W emulsion appears homogeneous after adjusting the solution pH to 7.5. Upon gradually decreasing the pH to 5.7, the oil droplets in the emulsion aggregate, lead to oil−water phase separation.

https://doi.org/10.1021/acsomega.4c00459
ACS Omega 2024, 9, 22691−22702

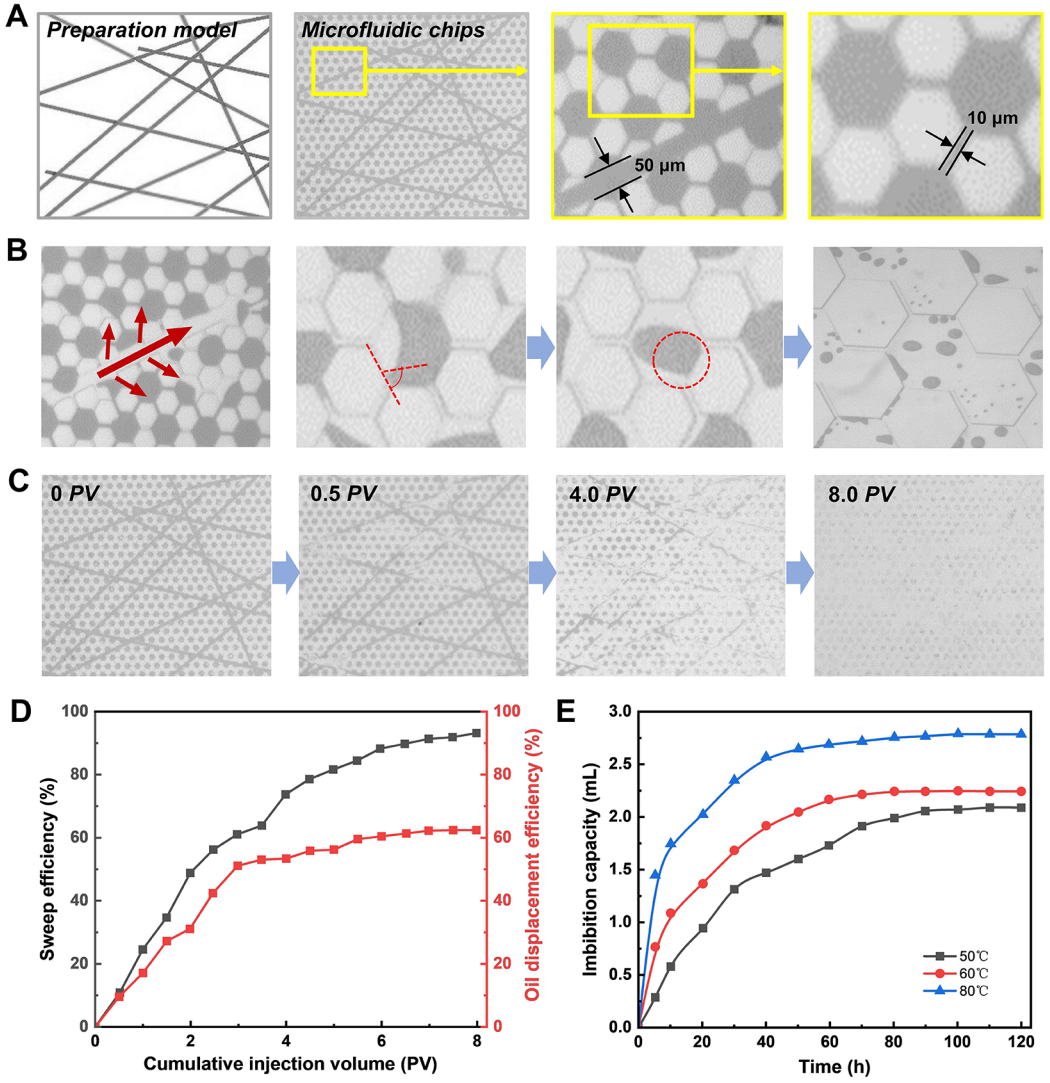

Figure 7. (A) Fabrication templates and microscopic characterization of microfluidic chips. (B) Real-time recorded images of microfluidic chip pore throat wetting transformation and oil droplet stripping process. (C) Real-time recorded images of the exfoliation process from a macroscopic viewpoint. (D) Cumulative sweep efficiency and oil displacement efficiency as a function of injection volume. (E) Variation curves of DOAPA/SA imbibition capacity with time at different temperatures.

However, upon adding NaOH solution to the demulsified oil−water mixture for 10 min, the system homogenizes and converts back into a stable oil−water emulsion. This process can be successfully repeated in subsequent demulsification and restabilization cycles. Additionally, room temperature storage for over 60 days without any treatment is achievable for the kerosene-in-water emulsion stabilized using 10 mM DOAPA/5 mM SA. This is explained by the fact that the self-assembly of the DOAPA/SA system is affected by the solution pH, resulting in emulsions that exhibit switchable behaviors and can undergo reversible emulsification and demulsification triggered by pH changes. These findings effectively demonstrate the sensitive response of the assembled surfactant (DOAPA/SA) to pH triggers and highlight the excellent reversibility of the switchable emulsification/demulsification behavior. Furthermore, this indicates the potential for pH adjustment to facilitate rapid demulsification of production fluids, hence eliminating the need for complex oil−water separation operations like static and ionization methods.[53,54]

3.5. Oil Displacement and Imbibition Capacity. The displacement and imbibition capacity measurement are also an important part of the performance evaluation of the fracturing and oil displacement integrated working fluid. In particular, the flowing state of the working fluid in the tiny pore structure of the formation and the interaction characteristics with oil, water, rock, and other substances largely determine the ability of the working fluid to enhance oil recovery. Here, taking a typical tight sandstone in unconventional reservoirs as an example, a new micromodel with pore throats and complex fracture networks was designed and fabricated to visually observe the flow behavior and action characteristics of DOAPA/SA fluids at the pore scale (Figure 7A). Figure 7B illustrates that the DOAPA/SA is injected into the leading edge and flanks in sufficient contact with the oil distributed in the fracture, the pore throats, and the narrow channels. Through the adsorption of surfactant molecules on the pore surface, the DOAPA/SA solution gradually alters the oil-wetting characteristic of the pore surface to water-wetting, causing the membranous flow to detach from the pore surface and form an oil-in-water emulsion. Its ability to thoroughly clean oil from tight pore spaces reaffirms the outstanding wetting and emulsifying properties of DOAPA/SA surfactants.

https://doi.org/10.1021/acsomega.4c00459
ACS Omega 2024, 9, 22691−22702

From the macroscopic point of view of Figure 7C, at the early stage of injection (0−0.5 PV), the flow resistance of fluid in the fracture is low, leading to the initial working fluid flowing along the fracture first, and the oil inside the fracture is driven first. In the middle stage of injection (0.5−4 PV), a large amount of oil in the pores and throats around the fracture is displaced, and the working fluid wave area gradually expands. However, in the middle stage of driving, a large amount of isolated residual oil and membranous residual oil remained in the wave area. Membrane residual oil refers to the residual oil attached to the fracture wall and pore corners. Isolated residual oil refers to the residual oil in the pores and throats separated by fractures. This is because in the tiny capillary pore channels, the contact area between the working fluid and the oil is small, and the advantage of high surface activity is difficult to act in a short time, making the driving force of the fluid into the tiny pores and throats lower, and then it is difficult to effectively displace the oil inside. It is noteworthy that the sweep volume of the working fluid was further expanded under the driving of the injection pressure, and there was no phenomenon of early breakthrough scuttling along the fracture. The statistical results in Figure 7D show that during the injection process of 0−8PV, the overall sweep efficiency and oil displacement efficiency reached 93.2% and 62.4%, respectively. The excellent sweep efficiency and oil displacement efficiency are attributed to the interfacial activity and viscoelastic properties of the DOAPA/SA system, which can effectively activate oil repulsion, drive the flow of residual oil, and control the breakthrough flow to increase the sweeping range.

In addition, it can be found from the imbibition curves in Figure 7E that the imbibition rate reaches the maximum value at the beginning of the experiment. Within 10 h after the start, DOAPA/SA spontaneously infiltrated into the core, and the range of the imbibition effect gradually expanded, and the imbibition rate decreased with the increase of time. In the range of 50−80 °C, which guarantees the stability of the rheological properties of the DOAPA/SA system, there is a significant increase in the imbibition rate and the final oil produced volume with the growth of the ambient temperature. At 80 °C, the imbibition capacity reached 2.79 mL and the extraction degree reached 19.86%. It was confirmed that the synergistic process of displacement and imbibition using the DOAPA/SA system can be used for the effective development of crude oil within tight reservoirs.

4. CONCLUSIONS

Based on the concept of integrated development of unconventional oil reservoirs, we have developed a pH-responsive viscoelastic solution system through the self-assembly surfactant. This system serves as an integrated working fluid for fracturing and oil displacement. The formula of the system consists of 240 mM DOAPA and 120 mM SA. Macroscopic rheological behavior and microscopic self-assembled structures of DOAPA/SA with pH-responsive properties. At pH 7.56, DOAPA and SA self-assemble to form wormlike micelles, producing a maximum viscosity of 93,100 mPa·s. By adjusting the pH, the zero-shear viscosity of the solution can be switched more than four times. The DOAPA/SA have excellent shear resistance and proppant carrying capacity, with viscosities above 500 mPa·s even after 60 min of shear at 80 °C and 170 s^{-1}. Moreover, the fracturing fluid can be easily broken within 1 h after adding kerosene, generating a low-viscosity liquid with no residue. The DOAPA/SA system had excellent interfacial activity, which can achieve reversible emulsification and demulsification through pH adjustment. Leveraging its viscoelastic properties and interfacial activity, DOAPA/SA effectively expands the swept volume and controls the breakthrough flow. Additionally, its high interfacial activity promotes pore-wetting transformation and facilitates the emulsification of residual oil, thereby enhancing oil-washing efficiency. The exceptional self-assembled viscoelastic gelation behavior and interfacial activity of DOAPA/SA present a novel approach for the development of integrated working fluids suitable for fracturing and displacement in unconventional oil reservoirs.

AUTHOR INFORMATION

Corresponding Authors

Xiaochen Li − *CNPC Bohai Drilling Engineering Company Limited, Tianjin 300280, People's Republic of China; Tianjin Enterprise Key Laboratory of Complex Conditions Drilling Fluid, Tianjin 300280, People's Republic of China; Unconventional Petroleum Research Institute, China University of Petroleum (Beijing), Beijing 102249, People's Republic of China;* orcid.org/0000-0002-7358-8226; Email: yuxiaodf@foxmail.com

Qiqi Niu − *Unconventional Petroleum Research Institute, China University of Petroleum (Beijing), Beijing 102249, People's Republic of China*; Email: nqq20202024@163.com

Authors

Xianbin Zhang − *CNPC Bohai Drilling Engineering Company Limited, Tianjin 300280, People's Republic of China; Tianjin Enterprise Key Laboratory of Complex Conditions Drilling Fluid, Tianjin 300280, People's Republic of China*

Leilei Wang − *CNPC Bohai Drilling Engineering Company Limited, Tianjin 300280, People's Republic of China; Tianjin Enterprise Key Laboratory of Complex Conditions Drilling Fluid, Tianjin 300280, People's Republic of China*

Fei Wen − *CNPC Bohai Drilling Engineering Company Limited, Tianjin 300280, People's Republic of China; Tianjin Enterprise Key Laboratory of Complex Conditions Drilling Fluid, Tianjin 300280, People's Republic of China*

Yurong Chen − *CNPC Bohai Drilling Engineering Company Limited, Tianjin 300280, People's Republic of China; Unconventional Petroleum Research Institute, China University of Petroleum (Beijing), Beijing 102249, People's Republic of China*

Qichao Lv − *Unconventional Petroleum Research Institute, China University of Petroleum (Beijing), Beijing 102249, People's Republic of China;* orcid.org/0000-0002-3270-5684

Hong Ma − *CNPC Bohai Drilling Engineering Company Limited, Tianjin 300280, People's Republic of China; Tianjin Enterprise Key Laboratory of Complex Conditions Drilling Fluid, Tianjin 300280, People's Republic of China*

Anliang Chen − *CNPC Bohai Drilling Engineering Company Limited, Tianjin 300280, People's Republic of China; Tianjin Enterprise Key Laboratory of Complex Conditions Drilling Fluid, Tianjin 300280, People's Republic of China*

Ruxue Wang − *CNPC Bohai Drilling Engineering Company Limited, Tianjin 300280, People's Republic of China; Tianjin Enterprise Key Laboratory of Complex Conditions Drilling Fluid, Tianjin 300280, People's Republic of China*

Leixu Chen − *CNPC Bohai Drilling Engineering Company Limited, Tianjin 300280, People's Republic of China; Tianjin*

https://doi.org/10.1021/acsomega.4c00459
ACS Omega 2024, 9, 22691−22702

Enterprise Key Laboratory of Complex Conditions Drilling Fluid, Tianjin 300280, People's Republic of China

Qian Wang − *CNPC Bohai Drilling Engineering Company Limited, Tianjin 300280, People's Republic of China; Tianjin Enterprise Key Laboratory of Complex Conditions Drilling Fluid, Tianjin 300280, People's Republic of China*

Dianbin Dong − *CNPC Bohai Drilling Engineering Company Limited, Tianjin 300280, People's Republic of China; Tianjin Enterprise Key Laboratory of Complex Conditions Drilling Fluid, Tianjin 300280, People's Republic of China*

Shaoying Xu − *CNPC Bohai Drilling Engineering Company Limited, Tianjin 300280, People's Republic of China; Tianjin Enterprise Key Laboratory of Complex Conditions Drilling Fluid, Tianjin 300280, People's Republic of China*

Complete contact information is available at: https://pubs.acs.org/10.1021/acsomega.4c00459

Author Contributions

Xiaochen Li: Conceptualization, Methodology, Article writing. Xianbin Zhang: Conceptualization, Methodology. Leilei Wang: Methodology, Project administration. Fei Wen: Methodology. Yurong Chen: Data curation. Qichao Lv: Conceptualization, Project administration. Hong Ma: Software. Anliang Chen: Data curation. Ruxue Wang: Formal analysis. Leixu Chen: Data curation. Qian Wang: Data curation. Dianbin Dong: Project administration. Shaoying Xu: Funding acquisition. Qiqi Niu: Conceptualization, Project administration, Article writing.

Notes

The authors declare no competing financial interest.

■ ACKNOWLEDGMENTS

This research was supported by the National Key Technologies R&D Program of China (2017ZX05009-004), the National Natural Science Foundation of China (52374056), and the Tianjin Science and Technology Program (19PTSYJC00120).

■ REFERENCES

(1) Muther, T.; Qureshi, H. A.; Syed, F. I.; Aziz, H.; Siyal, A.; Dahaghi, A. K.; Negahban, S. Unconventional hydrocarbon resources: geological statistics, petrophysical characterization, and field development strategies. *Journal of Petroleum Exploration and Production Technology* **2022**, *12* (6), 1463−1488.

(2) Jia, C.; Zheng, M.; Zhang, Y. Unconventional hydrocarbon resources in China and the prospect of exploration and development. *PETROLEUM EXPLORATION AND DEVELOPMENT* **2012**, *39* (2), 139−146.

(3) Chong, Z. R.; Yang, S. H. B.; Babu, P.; Linga, P.; Li, X.-S. Review of natural gas hydrates as an energy resource: Prospects and challenges. *APPLIED ENERGY* **2016**, *162*, 1633−1652.

(4) Jarvie, D. M.; Hill, R. J.; Ruble, T. E.; Pollastro, R. M. Unconventional shale-gas systems: The Mississippian Barnett Shale of north-central Texas as one model for thermogenic shale-gas assessment. *AAPG BULLETIN* **2007**, *91* (4), 475−499.

(5) Barati, R.; Liang, J.-T. A review of fracturing fluid systems used for hydraulic fracturing of oil and gas wells. *J. Appl. Polym. Sci.* **2014**, *131* (16), 40735.

(6) Montgomery, C. T.; Smith, M. B. Hydraulic Fracturing: History of an Enduring Technology. *Journal of Petroleum Technology* **2010**, *62* (12), 26−40.

(7) Vidic, R. D.; Brantley, S. L.; Vandenbossche, J. M.; Yoxtheimer, D.; Abad, J. D. Impact of Shale Gas Development on Regional Water Quality. *SCIENCE* **2013**, *340* (6134), 1235009.

(8) Davoodi, S.; Al-Shargabi, M.; Wood, D. A.; Rukavishnikov, V. S. A comprehensive review of beneficial applications of viscoelastic surfactants in wellbore hydraulic fracturing fluids. *Fuel* **2023**, *338*, No. 127228.

(9) Osiptsov, A. A. Fluid Mechanics of Hydraulic Fracturing: a Review. *JOURNAL OF PETROLEUM SCIENCE AND ENGINEERING* **2017**, *156*, 513−535.

(10) Ihejirika, B.; Dosunmu, A.; Eme, C., Performance Evaluation of Guar Gum as a Carrier Fluid for Hydraulic Fracturing. In *SPE Nigeria Annual International Conference and Exhibition*, 2015; pp SPE-178297-MS.

(11) Othman, A.; AlSulaimani, M.; Aljawad, M. S.; Sangaru, S. S.; Kamal, M. S.; Mahmoud, M. The Synergetic Impact of Anionic, Cationic, and Neutral Polymers on VES Rheology at High-Temperature. *Environment.* **2022**, *14* (6), 1145.

(12) Nsengiyumva, E. M.; Alexandridis, P. Xanthan gum in aqueous solutions: Fundamentals and applications. *Int. J. Biol. Macromol.* **2022**, *216*, 583−604.

(13) Wang, L.; Tian, Y.; Yu, X.; Wang, C.; Yao, B.; Wang, S.; Winterfeld, P. H.; Wang, X.; Yang, Z.; Wang, Y.; Cui, J.; Wu, Y.-S. Advances in improved/enhanced oil recovery technologies for tight and shale reservoirs. *FUEL* **2017**, *210*, 425−445.

(14) Weng, X.; Kresse, O.; Cohen, C.; Wu, R.; Gu, H. Modeling of Hydraulic-Fracture-Network Propagation in a Naturally Fractured Formation. *SPE PRODUCTION & OPERATIONS* **2011**, *26* (4), 368−380.

(15) Hurnaus, T.; Plank, J. Behavior of Titania Nanoparticles in Cross-linking Hydroxypropyl Guar Used in Hydraulic Fracturing Fluids For Oil Recovery. *Energy Fuels* **2015**, *29* (6), 3601−3608.

(16) Fink, J. K., Chapter 2 - Fluid Types. In *Hydraulic Fracturing Chemicals and Fluids Technology*; Fink, J. K., Ed.; Gulf Professional Publishing: 2013; pp 17−33.

(17) Yekeen, N.; Padmanabhan, E.; Idris, A. K.; Chauhan, P. S. Nanoparticles applications for hydraulic fracturing of unconventional reservoirs: A comprehensive review of recent advances and prospects. *JOURNAL OF PETROLEUM SCIENCE AND ENGINEERING* **2019**, *178*, 41−73.

(18) Kang, W.; Mushi, S. J.; Yang, H.; Wang, P.; Hou, X. Development of smart viscoelastic surfactants and its applications in fracturing fluid: A review. *JOURNAL OF PETROLEUM SCIENCE AND ENGINEERING* **2020**, *190*, 107107.

(19) Al-Muntasheri, G. A.; Liang, F.; Hull, K. L. Nanoparticle-Enhanced Hydraulic-Fracturing Fluids: A Review. *SPE PRODUCTION & OPERATIONS* **2017**, *32* (2), 186−195.

(20) Lu, Y.; Yang, F.; Ge, Z.; Wang, Q.; Wang, S. Influence of viscoelastic surfactant fracturing fluid on permeability of coal seams. *FUEL* **2017**, *194*, 1−6.

(21) Philippova, O. E.; Molchanov, V. S. Enhanced rheological properties and performance of viscoelastic surfactant fluids with embedded nanoparticles. *Curr. Opin. Colloid Interface Sci.* **2019**, *43*, 52−62.

(22) Davoodi, S.; Al-Shargabi, M.; Wood, D. A.; Rukavishnikov, V. S.; Minaev, K. M. Experimental and field applications of nanotechnology for enhanced oil recovery purposes: A review. *Fuel* **2022**, *324*, No. 124669.

(23) Pu, W.-f.; Du, D.-j.; Liu, R. Preparation and evaluation of supramolecular fracturing fluid of hydrophobically associative polymer and viscoelastic surfactant. *J. Pet. Sci. Eng.* **2018**, *167*, 568−576.

(24) Yang, Y.; Zhang, H.; Wang, H.; Zhang, J.; Guo, Y.; Wei, B.; Wen, Y. Pseudo-interpenetrating network viscoelastic surfactant fracturing fluid formed by surface-modified cellulose nanofibril and wormlike micelles. *J. Pet. Sci. Eng.* **2022**, *208*, No. 109608.

(25) Li, X.; Wang, P.; Hou, X.; Wang, F.; Zhao, H.; Zhou, B.; Zhang, H.; Yang, H.; Kang, W. Effects of sodium chloride on rheological behaviour of the gemini-like surfactants. *Soft Matter* **2020**, *16* (16), 4024−4031.

(26) Yang, X.; Mao, J.; Zhang, H.; Zhang, Z.; Zhao, J. Reutilization of thickener from fracturing flowback fluid based on Gemini cationic surfactant. *Fuel* **2019**, *235*, 670−676.

(27) Zhang, W.; Mao, J.; Yang, X.; Zhang, H.; Zhao, J.; Tian, J.; Lin, C.; Mao, J. Development of a sulfonic gemini zwitterionic viscoelastic

surfactant with high salt tolerance for seawater-based clean fracturing fluid. *Chem. Eng. Sci.* **2019**, *207*, 688−701.
(28) Mao, J.; Huang, Z.; Cun, M.; Yang, X.; Lin, C.; Zhang, Y.; Xu, T.; Zhang, H.; Du, A.; Wang, Q. Effect of spacer hydroxyl number on the performance of Gemini cationic viscoelastic surfactant for fracturing fluids. *J. Mol. Liq.* **2022**, *346*, No. 117889.
(29) Yan, Z.; Dai, C.; Zhao, M.; Sun, Y.; Zhao, G. Development, formation mechanism and performance evaluation of a reusable viscoelastic surfactant fracturing fluid. *JOURNAL OF INDUSTRIAL AND ENGINEERING CHEMISTRY* **2016**, *37*, 115−122.
(30) Huang, Q.; Liu, S.; Wang, G.; Cheng, W. Evaluating the changes of sorption and diffusion behaviors of Illinois coal with various water-based fracturing fluid treatments. *FUEL* **2021**, *283*, 118884.
(31) You, Q.; Wang, H.; Zhang, Y.; Liu, Y.; Fang, J.; Dai, C. Experimental study on spontaneous imbibition of recycled fracturing flow-back fluid to enhance oil recovery in low permeability sandstone reservoirs. *JOURNAL OF PETROLEUM SCIENCE AND ENGINEERING* **2018**, *166*, 375−380.
(32) Zeng, H.; Chen, L.; Chen, Y.; Li, G.; Mao, Z.; Liu, L. Research progress on fracturing-oil displacement integrated working fluid. *Petroleum Geology and Recovery Efficiency* **2022**, *29* (3), 162−170.
(33) Yan, J.; Li, Y.; Xie, X.; Slaný, M.; Dong, S.; Wu, Y.; Chen, G. Research of a novel fracturing-production integral fluid based on cationic surfactant. *J. Mol. Liq.* **2023**, *369*, No. 120858.
(34) Li, Z.; Kang, W.; Zhao, Y.; Yang, H.; Li, M.; Kang, X.; Zhu, T.; Zhou, B.; Sarsenbekuly, B.; Aidarova, S. Organic Acid-Enhanced Viscoelastic Surfactant and Its Application in Fracturing Fluids. *Energy Fuels* **2021**, *35* (4), 3130−3139.
(35) Herb, C. A.; Prud'homme, R. K. In *Structure and flow in surfactant solutions*, 1994.
(36) Israelachvili, J. N.; Mitchell, D. J.; Ninham, B. W. Theory of self-assembly of hydrocarbon amphiphiles into micelles and bilayers. *Journal of the Chemical Society, Faraday Transactions 2: Molecular and Chemical Physics* **1976**, *72* (0), 1525−1568.
(37) Yang, J. Viscoelastic wormlike micelles and their applications. *CURRENT OPINION IN COLLOID & INTERFACE SCIENCE* **2002**, *7* (5−6), 276−281.
(38) Sommer, C. Z. Structure and dynamics of charged worm-like micelles. Ph.D. Thesis, 2001.
(39) Candau, S. J.; Hebraud, P.; Schmitt, V.; Lequeux, F.; Kern, F.; Zana, R. Rheological behaviour of worm-like micelles: Effect of electrostatic interactions. *Il Nuovo Cimento D* **1994**, *16* (9), 1401−1410.
(40) Yang, Z.; Li, X.; Li, D.; Yin, T.; Zhang, P.; Dong, Z.; Lin, M.; Zhang, J. New Method Based on CO2-Switchable Wormlike Micelles for Controlling CO2 Breakthrough in a Tight Fractured Oil Reservoir. *ENERGY & FUELS* **2019**, *33* (6), 4806−4815.
(41) Kang, W.; Wang, P.; Fan, H.; Yang, H.; Dai, C.; Yin, X.; Zhao, Y.; Guo, S. A pH-responsive wormlike micellar system of a noncovalent interaction-based surfactant with a tunable molecular structure. *Soft Matter* **2017**, *13* (6), 1182−1189.
(42) Chu, Z.; Feng, Y. pH-switchable wormlike micelles. *Chem. Commun.* **2010**, *46* (47), 9028−9030.
(43) Molchanov, V. S.; Kuklin, A. I.; Orekhov, A. S.; Arkharova, N. A.; Philippova, O. E. Temporally persistent networks of long-lived mixed wormlike micelles of zwitterionic and anionic surfactants. *JOURNAL OF MOLECULAR LIQUIDS* **2021**, *342*, 116955.
(44) Holder, S. W.; Grant, S. C.; Mohammadigoushki, H. Nuclear Magnetic Resonance Diffusometry of Linear and Branched Wormlike Micelles. *Langmuir* **2021**, *37* (12), 3585−3596.
(45) Oelschlaeger, C.; Schopferer, M.; Scheffold, F.; Willenbacher, N. Linear-to-Branched Micelles Transition: A Rheometry and Diffusing Wave Spectroscopy (DWS) Study. *Langmuir* **2009**, *25* (2), 716−723.
(46) Kern, F.; Lequeux, F.; Zana, R.; Candau, S. J. Dynamic Properties of Salt-Free Viscoelastic Micellar Solutions. *Langmuir* **1994**, *10* (6), 1714−1723.
(47) Han, Y.; Feng, Y.; Sun, H.; Li, Z.; Han, Y.; Wang, H. Wormlike Micelles Formed by Sodium Erucate in the Presence of a Tetraalkylammonium Hydrotrope. *J. Phys. Chem. B* **2011**, *115* (21), 6893−6902.
(48) Kang, W.; Zhao, Y.; Wang, P.; Li, Z.; Hou, X.; Huang, Z.; Yang, H. Rheological behavior and mechanism of pH-responsive wormlike micelle variations induced by isomers of phthalic acid. *Soft Matter* **2018**, *14* (22), 4445−4452.
(49) Quan, H.; Zhang, X.; Lu, H.; Huang, Z. *Synthesis and acid solution properties of a novel betaine zwitterionic surfactant* **2012**, *10* (5), 1624−1632.
(50) Raghavan, S. R.; Kaler, E. W. Highly Viscoelastic Wormlike Micellar Solutions Formed by Cationic Surfactants with Long Unsaturated Tails. *Langmuir* **2001**, *17* (2), 300−306.
(51) Kruijf de, A. S.; Roodhart, L. P.; Davies, D. R. Relation Between Chemistry and Flow Mechanics of Borate-Crosslinked Fracturing Fluids. *SPE Production & Facilities* **1993**, *8* (03), 165−170.
(52) Castro Dantas, T. N.; Santanna, V. C.; Dantas Neto, A. A.; Curbelo, F. D. S.; Garnica, A. I. C. Methodology to break test for surfactant-based fracturing gel. *J. Pet. Sci. Eng.* **2006**, *50* (3), 293−298.
(53) Al-Ghouti, M. A.; Al-Kaabi, M. A.; Ashfaq, M. Y.; Da'na, D. A. Produced water characteristics, treatment and reuse: A review. *JOURNAL OF WATER PROCESS ENGINEERING* **2019**, *28*, 222−239.
(54) Das, N.; Rajput, H.; Hassan, A. A.; Kumar, S. Application of Different Coagulants and Cost Evaluation for the Treatment of Oil and Gas Produced Water. *WATER* **2023**, *15* (3), 464.

https://doi.org/10.1021/acsomega.4c00459
ACS Omega 2024, 9, 22691−22702